ELSEVIER

Journal of Photochemistry and Photobiology A: Chemistry 148 (2002) 85–89

Journal of Photochemistry and Photobiology A:Chemistry

www.elsevier.com/locate/jphotochem

Photocatalytic water decomposition by RuO_2-loaded antimonates, $M_2Sb_2O_7$ (M = Ca, Sr), $CaSb_2O_6$ and $NaSbO_3$, with d^{10} configuration

J. Sato, N. Saito, H. Nishiyama, Y. Inoue*

Department of Chemistry, Nagaoka University of Technology, Nagaoka 940-2188, Japan

Received 24 July 2001; received in revised form 11 September 2001; accepted 11 September 2001

Abstract

The photocatalytic activity for water decomposition of alkaline earth metal and alkaline metal antimonates, $M_2Sb_2O_7$ (M = Ca, Sr), $CaSb_2O_6$ and $NaSbO_3$, was investigated. These antimonates were photocatalytically active when combined with RuO_2: both H_2 and O_2 were produced from the initial stage of reaction under UV irradiation, and the photocatalytic activity became stable as the reaction proceeded. The photocatalytic properties are discussed based on the distorted structures of SbO_6 octahedra. © 2002 Elsevier Science B.V. All rights reserved.

Keywords: Photocatalysts; Water decomposition; Alkaline earth metal antimonates; Alkaline metal antimonates; The d^{10} configuration

1. Introduction

In previous studies, alkaline earth metal indates, MIn_2O_4 (M = Ca, Sr, Ba), were found to make stable photocatalysts for the decomposition of water to hydrogen and oxygen when combined with RuO_2 [1,2]. Furthermore, the preliminary studies of RuO_2-loaded Sr_2SnO_4 and $NaSbO_3$ showed that the stannate and the antimonate became photocatalytically active for water decomposition [2]. The interesting feature is that these metal oxides are composed of p-block metal ions (In^{3+}, Sn^{4+}, Sb^{5+}) with the octahedrally coordinated d^{10} metal ions.

A considerable number of solid photocatalysts for the overall splitting of water has been discovered in extensive research. In most cases, the photocatalysts are formed by the combination of transition metal oxides and promoters. The former has the function to generate the photoexcited charges, whereas the latter, usually fine Pt, NiO or RuO_2 particles dispersed on the metal oxides, plays a role in the transfer of the charges to the surfaces where the reduction and the oxidation of adsorbed species occur. The representative metal oxides reported in the past two decades are schematically shown in Fig. 1. They are $SrTiO_3$ [3], $A_2Ti_6O_{13}$ (A = Na, K, Rb) [4,5], $BaTi_4O_9$ [6,7], $A_2La_2Ti_3O_{10}$ (A = K, Rb, Cs) [8,9], $Na_2Ti_3O_7$ [10], $K_2Ti_4O_9$ [11], ZrO_2 [12], $A_4Nb_6O_{17}$ (A = K, Rb) [13], $Sr_2Nb_2O_7$ [14], $ATaO_3$ (A = Na, K) [15,16], MTa_2O_6 (M = Ca, Sr, Ba) [17,18] and $Sr_2Ta_2O_7$ [14].

It should be noted that some of the metal oxides have complicated crystal structures and offer highly active photocatalysis. For examples, $A_4Nb_6O_{17}$ (A = K, Rb) has two kinds of layers with anisotropy along the stacking direction [13]. $BaTi_4O_9$ and $A_2Ti_6O_{13}$ (A = Na, K, Rb) are characterized by tunnel structures formed by heavily distorted TiO_6 octahedra [19–21]. The distorted structures of metal–oxygen (M–O_6) octahedra are proposed to be responsible for efficient photoexcitation and charge separation. In spite of the employment of different type transition metal oxides, it should be noted that the core elements of Ti^{4+}, Zr^{4+}, Nb^{5+} and Ta^{5+} are octahedrally coordinated d^0 transition metal ions. The previous discovery that the p-block metal oxides with d^{10} configuration are active for water decomposition suggests the possibility of establishing of a new photocatalyst group with different electronic structures. For this purpose, it is of importance to perform extensive research for the photocatalytic properties of the p-block metal oxides.

In the present study, the photocatalytic activity by alkaline earth metal and alkaline metal antimonates with octahedrally coordinated d^{10} Sb^{5+} ion was examined. $M_2Sb_2O_7$ (M = Ca, Sr), $CaSb_2O_6$ and $NaSbO_3$ were chosen, and their photocatalytic behavior for water decomposition was investigated in detail. The combination with RuO_2 was found to form active photocatalysts that have the capability of producing H_2 and O_2. The role of local structure of

* Corresponding author. Tel.: +81-258-47-9832; fax: +81-258-47-9830.
E-mail address: inoue@analysis.nagaokaut.ac.jp (Y. Inoue).

1010-6030/02/$ – see front matter
PII: S1010-6030(02)00076-X

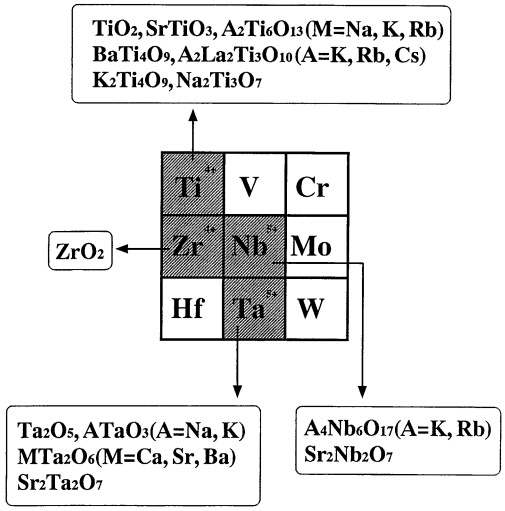

Fig. 1. Octahedrally coordinated d^0 transition metal ions and their representative transition metal oxide group photocatalytically active for water decomposition when combined with promoters.

SbO_6 octahedra is discussed based on the correlation of their crystal structures with photocatalytic activity.

2. Experimental

In the synthesis of $M_2Sb_2O_7$ (M = Ca, Sr) and $CaSb_2O_6$, a molar ratio mixture of Sb_2O_3 (Merck, 99% pure) and $CaCO_3$ (Junsei Chemical Co., GR grade) or $SrCO_3$ (Kanto Chemical Co., GR grade) was calcined in air at 1373 K in air for 16 h. $NaSbO_3$ was prepared by calcination of a 1:1 molar mixture of Na_2CO_3 (Nacalai Tesque Inc., GR grade) and Sb_2O_3 in air at 1173 K for 16 h. The formation of the metal oxides was confirmed by their X-ray diffraction patterns. The p-block metal oxides thus prepared were impregnated up to incipient wetness with a ruthenium carbonyl complex, $Ru_3(CO)_{12}$ (Aldrich Chemical Co., 99% pure), in tetrahydrofuran, dried at 353 K and oxidized to produce RuO_2 in air at 673 K for 5 h. The photocatalytic reaction was carried out in a closed gas circulating reaction apparatus with a piston pump. About 250 mg of powder photocatalysts was placed in a quartz reaction cell filled with ca. 20 cm^3 of distilled and ion-exchanged water. Ar gas of 13.3 kPa was circulated with the piston pump during the reaction. The powder photocatalysts were dispersed in the water by stirring of Ar gas bubbling and illuminated by a Hg–Xe lamp operated at 200 W. The lamp had emission lines in the wavelength range of 248–643 nm. The evolved gases were analyzed by a gas chromatograph connected to the reaction system. The light absorption characteristics of the antimonates were obtained on a UV reflectance spectrometer (JASCO UVIDEC-660). X-ray photoelectron spectra were recorded on a JEOL JPS-100SX spectrometer using Al Kα. The binding energy was corrected by taking C 1s level as 284.6 eV.

3. Results

Fig. 2a shows water decomposition on 1 wt.% RuO_2-loaded $Ca_2Sb_2O_7$ under Hg–Xe lamp irradiation. In the initial stage of the first run, the evolution of H_2 was initially fast, followed by a gradual decrease as the reaction proceeded, whereas oxygen was produced in nearly linear manner with reaction time. The reaction was repeated by evacuating gas phase products, and good reproducibility of both H_2 and O_2 production was observed for the second to the fourth run. In the fourth run, the production of H_2 and O_2 over time was linear manner with reaction time. As shown in Fig. 2b, for 1 wt.% RuO_2-loaded $Sr_2Sb_2O_7$, H_2 and O_2 production was in nearly proportion to irradiation time from the initial stage, and stable and reproducible evolution was observed through the first to the fourth run. Little deterioration of the photocatalytic efficiency was observed for both RuO_2-loaded $Ca_2Sb_2O_7$ and $Sr_2Sb_2O_7$. Fig. 3 shows the repetition of reaction on 1 wt.% RuO_2-loaded $NaSbO_3$. In the first run, extraordinary large evolution of H_2 occurred, whereas O_2 production showed an induction period. In the second and third run, however, both H_2 and O_2 were produced at a constant rate, attaining at steady state

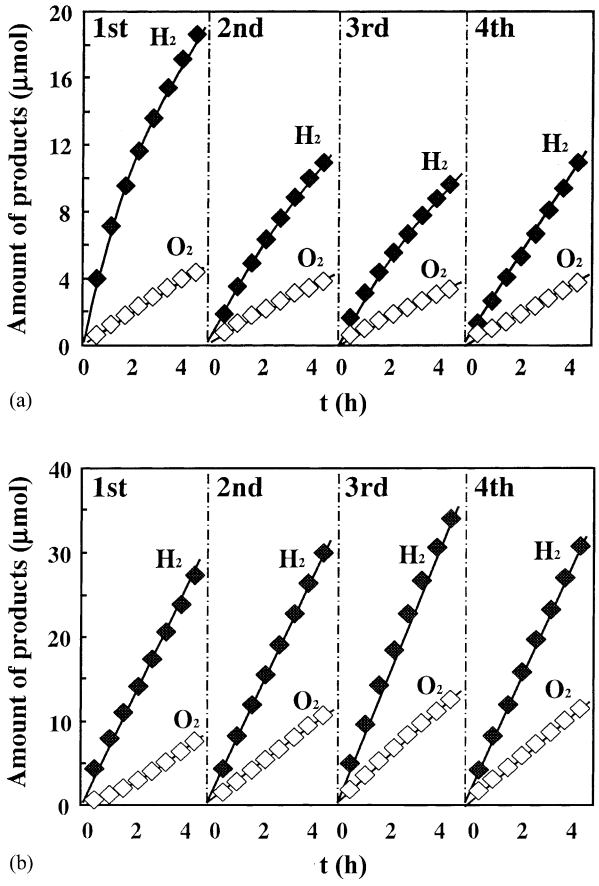

Fig. 2. Photocatalytic water decomposition on (a) 1 wt.% RuO_2-loaded $Ca_2Sb_2O_7$ and (b) 1 wt.% RuO_2-loaded $Sr_2Sb_2O_7$. The photocatalytic reaction was repeated four times by evacuating the products in gas phase.

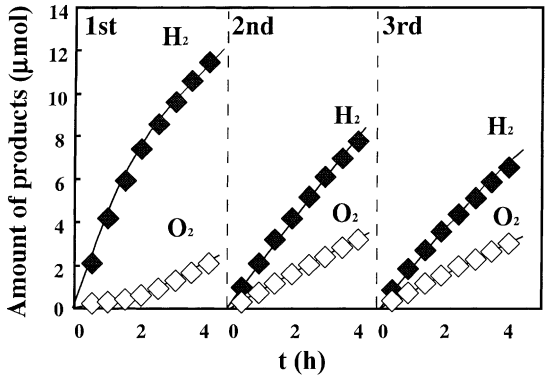

Fig. 3. Evolution of H_2 and O_2 on 1 wt.% RuO_2-loaded $NaSbO_3$. The photocatalytic reaction was repeated three times by evacuating the products in gas phase.

conditions. Little production of H_2 and O_2 was observed for the antimonates in the absence of RuO_2.

Fig. 4 shows the UV diffuse reflectance spectra of $M_2Sb_2O_7$ (M = Ca, Sr), $NaSbO_3$ and $CaSb_2O_6$. Light absorption of $Ca_2Sb_2O_7$ began at around 380 nm and attained the maximum level at 280 nm. The absorption characteristics of $Sr_2Sb_2O_7$ were quite similar to that of $Ca_2Sb_2O_7$ except for slightly shorter onset wavelength. For $NaSbO_3$, abrupt absorption occurred at around 280 nm. For $CaSb_2O_6$, the absorption occurred gradually at abound 400 nm, and the main absorption was similar to that of $M_2Sb_2O_7$ (M = Ca, Sr).

Fig. 5 shows X-ray photoelectron spectrum of $Sr_2Sb_2O_7$ in the binding energy range 0–50 eV. A sharp peak of Sb 4d level appeared at 34.2 eV. The Sr 4s and Sr 4p levels were observed at 24.2 and 18.2 eV, respectively. A broad peak near the valence band was due to the O 2p level. It is interesting to note that the Sb 4d level is located at a deep inner level from the valence band.

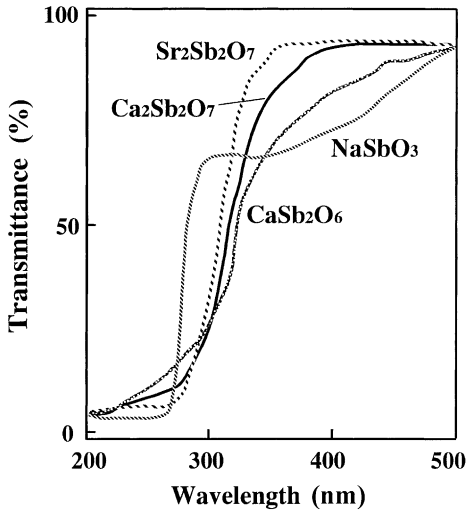

Fig. 4. UV diffuse reflectance spectra of $M_2Sb_2O_7$ (M = Ca, Sr), $NaSbO_3$ and $CaSb_2O_6$.

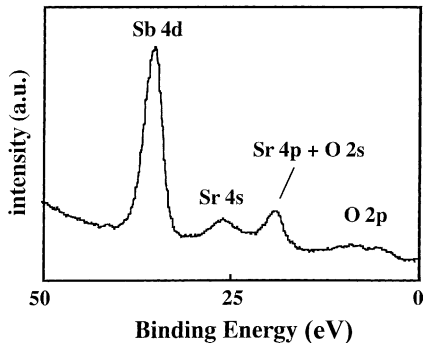

Fig. 5. X-ray photoelectron spectrum of $Sr_2Sb_2O_7$.

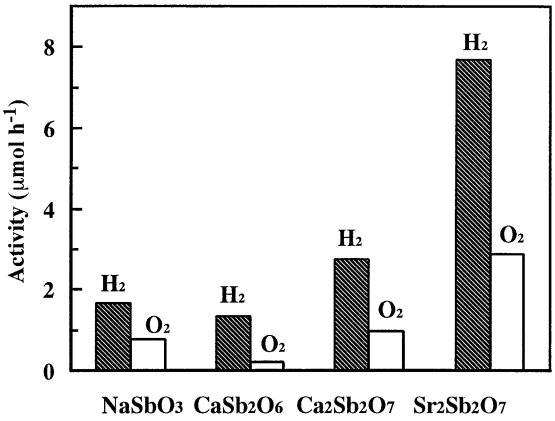

Fig. 6. Photocatalytic activity of 1 wt.% RuO_2-loaded $M_2Sb_2O_7$ (M = Ca, Sr), $NaSbO_3$ and $CaSb_2O_6$.

Fig. 6 shows the photocatalytic activity of 1 wt.% RuO_2-loaded $M_2Sb_2O_7$ (M = Ca, Sr), $NaSbO_3$ and $CaSb_2O_6$. Under similar reaction conditions, the activity of RuO_2-loaded $Sr_2Sb_2O_7$ was the greatest of the four antimonates tested: the activity was greater by a factor of 2.8 compared with that of the RuO_2-loaded $Ca_2Sb_2O_7$, and by a factor of 4.7 compared with that of the RuO_2-loaded $NaSbO_3$ and by a factor of 5.9 compared with that of the RuO_2-loaded $CaSb_2O_6$.

4. Discussion

The production of H_2 and O_2 from water was clearly observed for RuO_2-loaded $M_2Sb_2O_7$ (M = Ca, Sr) under UV irradiation. The repetition of reaction run showed that the photocatalysts changed to show better performance for the decomposition of water and to become stable. Similar reaction behavior in the repetition of reaction was observed for RuO_2-loaded $NaSbO_3$. These results indicate that RuO_2-loaded antimonates have the capability to photocatalytically decompose water, to produce H_2 and O_2, under UV illumination.

The photocatalytic activity of RuO_2-loaded $M_2Sb_2O_7$ (M = Ca, Sr) was larger for M = Sr than M = Ca. This is the opposite to the order of activity previously reported for RuO_2-loaded MIn_2O_4 (M = Ca, Sr, Ba) and M_2SnO_4 (M = Ca, Sr, Ba) for which the activity increased in the order Ca > Sr ≫ Ba [22]. In the SEM observation, the particle size of M_2SnO_4 (M = Ca, Sr, Ba) was similar among three stannates, but the particle size of $M_2Sb_2O_7$ (M = Ca, Sr) was significantly different between $Ca_2Sb_2O_7$ and $Sr_2Sb_2O_7$. $Ca_2Sb_2O_7$ exhibited large particles whose average particle size was about 5 μm. The large particles were formed by agglomeration of fine particles as small as 0.5 μm. On the other hand, $Sr_2Sb_2O_7$ had fine particles whose average particle size was 0.3 μm. Thus, it is likely that the reverse activity order is associated with the macroscopic morphological differences.

Fig. 7 shows the schematic representation of the structure of $M_2Sb_2O_7$ (M = Ca, Sr). This compound has a weberite structure consisting of two kinds of SbO_6 octahedra. One type $SbO_6(1)$ is connected to surrounding four octahedra, and the other type $SbO_6(2)$ is connected to six octahedral [23]. As shown in Fig. 7, $SbO_6(1)$ has two shorter Sb–O bonds, compared to the remaining four bonds with the same bond length, thus forming compressed octahedron. In contrast, $SbO_6(2)$ has two longer Sb–O bonds, forming elongated octahedron. Fig. 8 shows $NaSbO_3$ with ilmenite structure. $NaSbO_3$ contains alternating layers of edge-sharing SbO_6 octahedra [24]. The SbO_6 octahedron is distorted in such a way that the Sb ion is in the out-of-center position. $CaSb_2O_6$ is composed of infinite sheets of edge-sharing SbO_6 octahedra alternating with layers of Ca ion [25]. The octahedra are stretched in the one plane and are contracted in the other direction, forming distortion. It should be noted that all the antimonates with deformed SbO_6 octahedra induce the photocatalytic activity when combined with RuO_2. In our recent study of RuO_2-loaded stannates, M_2SnO_4 (M = Ca, Sr, Ba), the photocatalytic activity was remarkably large for M = Ca and Sr, whereas little activity was observed for M = Ba [22]. The crystal structure analysis showed that the SnO_6 octahedra of Ca_2SnO_4 and Sr_2SnO_4 were distorted, whereas Ba_2SnO_4 had normal SnO_6 octahedra. Based on these results, it is rationally assumed that deformed SnO_6 octahedra play an important role in the generation of photocatalysis by the stannates. Furthermore, in previous studies of photocatalysis by RuO_2-loaded various titanates with octahedrally coordinated d^0 configuration, the involvement of the local structure in the photocatalytic properties of the titanates has been demonstrated. The pentagonal prism tunnel structure of $BaTi_4O_9$ and the rectangular tunnel of $A_2Ti_6O_{13}$ (A = Na, K, Rb) are composed of heavily distorted TiO_6 octahedra [19–21]. The out-of-center Ti ions are proposed to have significant effects on the formation of photoexcited charges, since a stable radical was observed for the tunnel structure titanates by the EPR signal when irradiated with UV light at 77 K in the presence of gaseous molecules such as Ar, He, O_2 and H_2 [26,27]. The photocatalytic activity of RuO_2-loaded $BaTi_4O_9$ and $A_2Ti_6O_{13}$ (A = Na, K, Rb) was associated with the radical concentration, indicating that the distorted TiO_6 octahedra of the tunnel structures promote the photoexcitation [28]. The same results were also obtained for layer structure titanates such as $Na_2Ti_3O_7$ and $K_2Ti_4O_9$ [10,11]. These results lead to a view that the deformed $M–O_6$ octahedra have a significant effect in photocatalysis. It appears, however, that there is a difference in the effect of octahedral deformation between the p-block and the transition metal octahedra. For the p-block metal oxides, the effect is significant even when the extent of distortion is

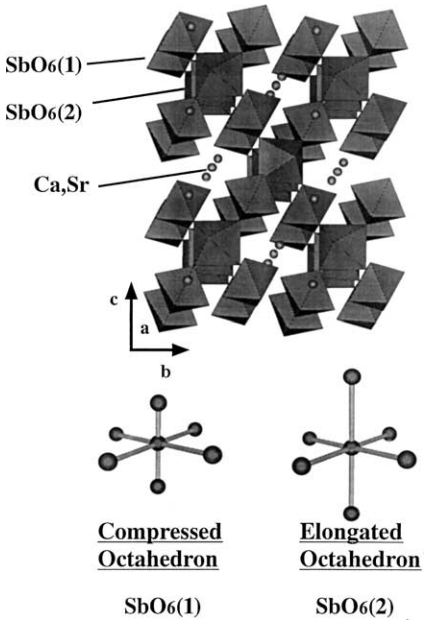

Fig. 7. Schematic representation of weberite structure of $M_2Sb_2O_7$ (M = Ca, Sr) and two kinds of SbO_6 octahedra.

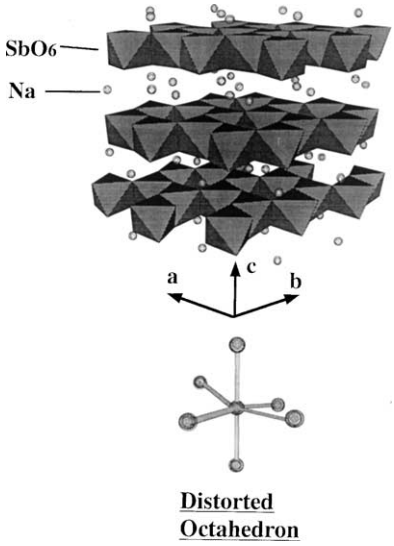

Fig. 8. Schematic representation of ilmenite structure of $NaSbO_3$ and a distorted SbO_6 octahedron.

small, whereas for the transition metal oxides such as the titanates, the deformation was large enough to produce dipole moment in their octahedra. It is likely that the difference in the deformation effect on photocatalysis is associated with the nature of chemical bonds where photoexcitation is involved.

For the active metal oxides for the overall splitting of water, the comparison of the d^0 transition metal oxides and the d^{10} p-block metal oxides leads to an interesting view that both electronic structures of completely empty and filled d orbitals are associated with the generation of photocatalytic activity. In the d^0 Ti metal oxides, the conduction bands are formed by the empty d orbital, whereas the valence bands are formed by the O 2p orbital. The X-ray photoelectron spectra of $Ca_2Sb_2O_7$ showed that the Sb 4d level was present at around 34 eV below the valence band of the O 2p level. Remarkable stability of d band is characteristic of p-block metal oxides and is due to an increase in the nuclear charges. Since the Sb 4d orbital is regarded as deep core levels, it follows that the valence bands of the antimonates are essentially composed of the O 2p orbital. The situation with the valence band is the same as that in the d^0 transition metal oxides. However, the nature of the conduction band is completely different, which appears to be responsible for the differences in deformation effects on photoexcitation and photocatalytic activity. Although the antimonates employed here have light absorption only in the UV region, the interesting features of p-block metal oxides are that their light absorption characteristics strongly depend on their chemical compositions and structures. This is likely to be associated with the nature of the conduction band, suggesting the possibility of development of p-block metal oxide photocatalysts working under visible light region.

In conclusion, the present study clearly shows that RuO_2-combined alkaline earth metal and alkaline metal antimonates are new photocatalysts that have the capability of decomposing water to H_2 and O_2 under UV illumination.

Acknowledgements

This work was supported by CREST of JSP.

References

[1] J. Sato, N. Saito, H. Nishiyama, Y. Inoue, Chem. Lett., (2001) 868–869.
[2] J. Sato, N. Saito, H. Nishiyama, Y. Inoue, J. Phys. Chem. 105 (2001) 6061–6063.
[3] K. Domen, A. Kudo, T. Onishi, J. Catal. 102 (1986) 92–98.
[4] Y. Inoue, T. Kubokawa, K. Sato, J. Phys. Chem. 95 (1991) 4059–4063.
[5] S. Ogura, M. Kohno, K. Sato, Y. Inoue, Appl. Surf. Sci. 121/123 (1997) 521–524.
[6] Y. Inoue, Y. Asai, K. Sato, J. Chem. Soc., Faraday Trans. 90 (1994) 797–802.
[7] M. Kohno, T. Kaneko, S. Ogura, K. Sato, Y. Inoue, J. Chem. Soc., Faraday Trans. 94 (1998) 89–94.
[8] T. Takata, Y. Furumi, K. Shinohara, A. Tanaka, M. Hara, J.N. Kondo, K. Domen, Chem. Mater. 9 (1997) 1063–1064.
[9] T. Takata, K. Shinohara, A. Tanaka, M. Hara, J.N. Kondo, K. Domen, J. Photochem. Photobiol. A: Chem. 106 (1997) 45–49.
[10] S. Ogura, M. Kohno, K. Sato, Y. Inoue, J. Mater. Chem. 8 (1994) 2335–2337.
[11] S. Ogura, K. Sato, Y. Inoue, Phys. Chem. Chem. Phys. 2 (2000) 2449–2454.
[12] K. Sayama, H. Arakawa, J. Phys. Chem. 97 (1993) 531–533.
[13] A. Kudo, A. Tanaka, K. Domen, K. Maruya, K. Aika, T. Onishi, J. Catal. 111 (1998) 67–76.
[14] A. Kudo, H. Kato, S. Nakagawa, J. Phys. Chem. B 104 (2000) 571–575.
[15] H. Kato, A. Kudo, Catal. Lett. 58 (1999) 153–155.
[16] T. Ishihara, H. Nishiguchi, K. Fukamachi, Y. Takita, J. Phys. Chem. B 103 (1999) 1–3.
[17] H. Kato, A. Kudo, Chem. Phys. Lett. 295 (1998) 487–492.
[18] H. Kato, A. Kudo, Chem. Lett. (1999) 1207–1208.
[19] W. Hofmeister, E. Tillmanns, W.H. Bauer, Acta Cryst. C40 (1984) 1510–1512.
[20] D.H. Templeton, C.H. Dauben, J. Chem. Phys. 32 (1960) 1515–1518.
[21] S. Andersson, A.D. Wadsley, Acta Cryst. 15 (1962) 194–199.
[22] J. Sato, N. Saito, H. Nishiyama, Y. Inoue, Unpublished data.
[23] W.A. Groen, D.J.W. Ijdo, Acta Cryst. C44 (1988) 782–784.
[24] B.G. DeBoer, R.A. Young, A. Sakthivel, Acta Cryst. C50 (1994) 476–482.
[25] B. Wang, S.C. Chen, M. Greenblatt, J. Solid State Chem. 108 (1994) 184–188.
[26] M. Kohno, S. Ogura, K. Sato, Y. Inoue, Chem. Phys. Lett. 267 (1997) 72–76.
[27] S. Ogura, M. Kohno, K. Sato, Y. Inoue, Phys. Chem. Chem. Phys. 1 (1999) 179–183.
[28] S. Ogura, M. Kohno, K. Sato, Y. Inoue, J. Chem. Soc., Faraday Trans. 93 (1997) 2433–2437.